Effect of point defects on the thermal transport properties of $(La_xGd_{1-x})_2Zr_2O_7$: Experiment and theoretical model

C. L. Wan, W. Pan,* Q. Xu, Y. X. Qin, J. D. Wang, Z. X. Qu, and M. H. Fang
State Key Laboratory of New Ceramics and Fine Processing, Department of Materials Science and Engineering, Tsinghua University, Beijing, 100084, China

(Received 13 June 2006; revised manuscript received 21 August 2006; published 30 October 2006)

Thermal transport properties of solid solution $(La_xGd_{1-x})_2Zr_2O_7$ have been investigated for thermal barrier coatings (TBCs) application. The introduction of point defects was intended to provide extra phonon scattering, and much lower thermal conductivity for the solid solution has been obtained compared with $La_2Zr_2O_7$ and $Gd_2Zr_2O_7$. The phonon mean free paths of the solid solution were estimated and discussed with respect to the point defect scattering effect. Young's modulus and heat capacity of the solid solution, which determine the mean velocity and the carried energy of the phonons, respectively, were measured and both showed suppression compared with the end materials, possibly due to the lattice relaxation aroused by point defects. A theoretical model, which contains no adjustable parameters, was present to accurately describe the thermal conductivities of the solid solution by taking account of the mass and strain field fluctuations induced by the point defects.

DOI: 10.1103/PhysRevB.74.144109 PACS number(s): 63.20.Mt, 65.40.Ba

I. INTRODUCTION

Thermal barrier coatings (TBCs) have been developed to protect and insulate the hot section of the metallic components in gas turbine and increase the engine inlet gas temperature, resulting in significant improvements in thermal efficiency, performance, and reliability.[1–5] Therefore, low thermal conductivity has been the critical parameter for materials applied in TBCs. Yttria stabilized zirconia (YSZ),[1–4] which has been almost universally used, relies mostly on oxygen vacancies to provide necessary phonon scattering for low thermal conductivity (2.0 W/mK, 700 °C) and much of its physics has been investigated.[6,7] Meanwhile, the microstructure in the coating layer including the micropore, the crystal size and orientation has been optimized for better thermal insulation property as well as better reliability and durability.[8,9] In recent years, there is considerable interest in developing TBCs with even lower thermal conductivity and chemical stability at higher temperature to achieve further improvements in engine performance. Among thousands of possible refractory compounds, rare-earth elements doping zirconates with a general formula of $R_2Zr_2O_7$ (where R is La, Nd, Gd, Sm, Er, Dy, Yb,…) have been selected as promising candidates for a new generation of TBCs. The class of materials which crystallize in pyrochlore or defect fluorite structure involve large content of structural oxygen vacancies in the unit cell, giving rise to strong phonon scattering and reduced thermal conductivity. It has been reported that the thermal conductivities for zirconates doped with Gd, Eu, Sm, Nd, Er, Dy, Yb, and La range from 1.1 W/mK to 1.8 W/mK at temperatures between 700 °C and 1200 °C,[10–15] and an MD study has recently been performed on this class of materials, which provides some insight into their thermal conductivities as well as elastic properties and thermal expansion coefficients.[16] Codoping of pyrochlores on both A and B sites has been proposed to further reduce their conductivity and also to modify their thermal expansion coefficients.[17,18] Lehmann *et al.*[17] reported their results in which $La_2Zr_2O_7$ was doped with 30 at. % of Nd, Eu, or Gd and the thermal conductivity was further reduced from ~1.55 W/mK to ~0.9 W/mK at 800 °C for Gd doping. Meanwhile, the phonon scattering mechanism for the doped fluorite and pyroclore structured oxide materials have been discussed theoretically using solid physics and crystal chemistry recently.[12,17]

In the present work, we introduce additional point-defect phonon scattering into $R_2Zr_2O_7$ by forming solid solution $(R1_xR2_{1-x})_2Zr_2O_7$ (R, $R1$, and $R2$ represent different Lanthanide elements, respectively), in order to find materials with even lower thermal conductivity while keeping good chemical stability. The selected components for the solid solution were $Gd_2Zr_2O_7$ and $La_2Zr_2O_7$, according to the fact that $Gd_2Zr_2O_7$ nearly possesses the lowest thermal conductivity among the lanthanide zirconates.[19] Lanthanum with large ionic radius was added to introduce significant lattice distortion, which serves as strong phonon scattering sources. In Lehmann *et al.*'s work,[17] one composition of $(La_{0.7}Gd_{0.3})_2Zr_2O_7$ has been studied, but a systematic research across the whole composition range is necessary both for practical and theoretical significance, such as searching for compositions with even lower thermal conductivity and providing guidance for other similar systems.

In addition, phonon mean free path, Young's modulus, and heat capacities of the solid solution were calculated and measured to clarify the effect of point defects on the thermal transport properties and its underlying physics. We also present a theoretical model to describe the thermal conductivity of the solid solution by taking account of the mass fluctuations and stain field fluctuations for better understanding of phonon scattering mechanism by point defects.

II. EXPERIMENTAL DETAILS

The $(La_{1-x}Gd_x)_2Zr_2O_7$ $(x=0,1/6,1/3,1/2,2/3,5/6,1)$ specimens were synthesized by the coprecipitation method.[20]

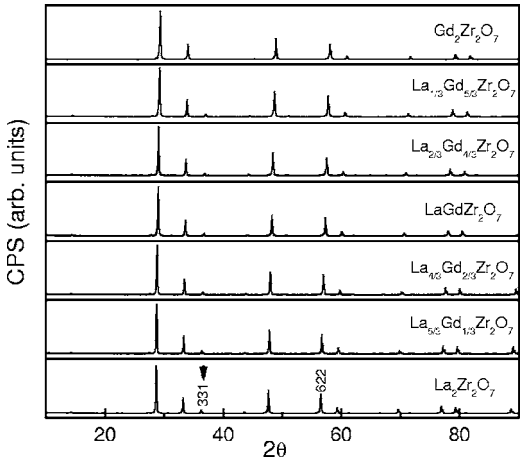

FIG. 1. XRD patterns of $(La_{1-x}Gd_x)_2Zr_2O_7$ ($x=0,1/6,1/3,1/2,2/3,5/6,1$).

For each composition Gd_2O_3 (purity 99.9%, Rear Earth Chem. Co. China) and La_2O_3 (99.9%, Rear Earth Chem. Co. China) were weighted, dissolved in acid, and mixed with $ZrOCl_2$ (99%, Rear Earth Chem. Co. China) solution. La_2O_3 was calcined at 1000 °C for 6 h before weighting for absorption of water. The mixed solution was slowly added into excessive ammonia water (pH > 10.5) with mechanical and ultrasonic agitating. The precipitates were then washed and filtered for several times to pH 7. The precursor powder was ground and calcined at 800 °C for 5 h for crystallization. The powder acquired was dry-pressed into the disk shape and sintered at 1600 °C for 20 h. The phases of the sintered bulk materials were then characterized by x-ray diffraction (D/max-RB, Japan), and the microstructure of the specimen was observed by scanning electron microscopy (SEM, Jeol-6301F, Japan). The density $\rho(g/cm^3)$ of the sintered bulk specimen was measured according to Archimedes principle. The theoretical densities of each solid solution composition were calculated using lattice parameters acquired from XRD result and the molecular weight contained in one elementary cell. The atomic structure of $LaGdZr_2O_7$ was observed by high resolution transmission microscope (HRTEM, JEM-2010, Japan) operating at 200 KV. Thermal diffusivity (κ) was measured using the laser-flash method (NETZSCH LFA 427, Germany). Specific heat capacity of the specimen, C_P, was measured by DSC instrument (NETZSCH DSC204, Germany). Thermal conductivity of the sintered specimen was then determined using the formula:

$$k' = \kappa \cdot C_P \cdot \rho. \tag{1}$$

Since the sintered specimen still contains some micropore, thermal conductivity of the full dense solid (k) was further normalized by the formula:[21]

$$\frac{k'}{k} = 1 - \frac{4}{3}\phi, \tag{2}$$

where ϕ is the porosity of the sintered specimen. The longitudinal and transverse acoustic velocities were measured by an ultrasonic instrument (Ultrasonic Pulser/Recever Model 5900 PR, Panametrics, USA) and the elastic constants and Poisson ratio were then calculated from the measured velocities.[22] These values of elastic constants were extrapolated to full density by the formula:[22]

$$E_0 = E(\phi)/(1-\phi^{2/3})^{1.21}. \tag{3}$$

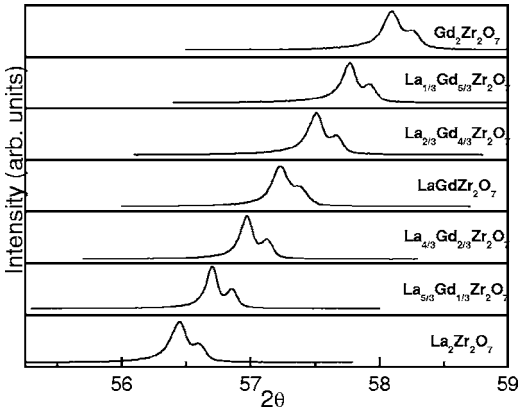

FIG. 2. The shift of the (662) peak with the substitution of La^{3+} by Gd^{3+} in $La_2Zr_2O_7$.

III. RESULTS

A. Structure analysis

Figure 1 reveals the x-ray diffraction patterns of synthesized $(La_{1-x}Gd_x)_2Zr_2O_7$ specimens. It can be found that the single-phase materials were obtained for all the compositions. $Gd_2Zr_2O_7$ exhibits a defect fluorite-type structure, and with the incorporation of larger La^{3+}, it transformed into an ordered pyrochlore-type structure, which is consistent with several other $A_2B_2O_7$-type solid solutions.[23] The (331) peak characterizes the superstructure of the ordered pyrochlore-type structure and it can be used to distinguish between pyrochlore and fluorite structure.[23]

Fine stepwise x-ray diffraction on single peak (622) has been conducted and regular displacement of the peak against the composition variation was observed (Fig. 2). A linear change of the lattice parameters with composition of the solid solution is shown in Fig. 3, which is in agreement with Vegard's rule.[24] The result indicates that Gd^{3+} is displaced by

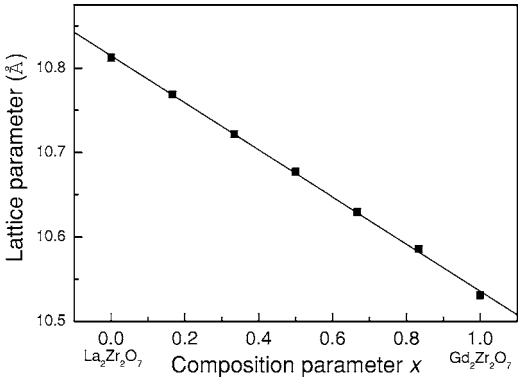

FIG. 3. Lattice parameters of $(La_{1-x}Gd_x)_2Zr_2O_7$.

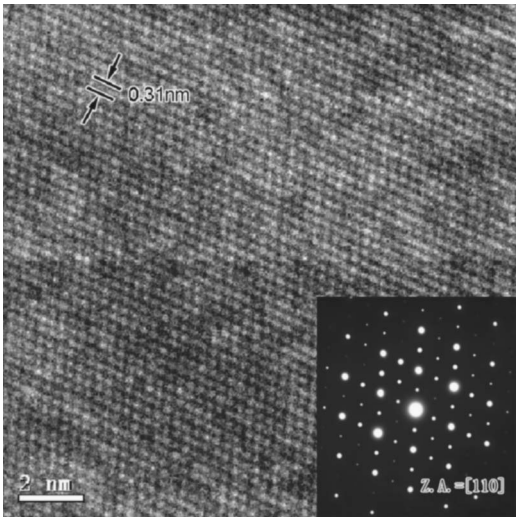

FIG. 4. HRTEM image of $LaGdZr_2O_7$ along the (110) zone axis.

La^{3+} or Gd^{3+} has taken the site of La^{3+}, and the infinite solid solution of lanthanum-gadolinium zirconate has formed. An HRTEM image of $LaGdZr_2O_7$ along the (110) zone axis is present in Fig. 4. The selected area electron diffraction (SAED) pattern confirms that $LaGdZr_2O_7$ possesses a pyrochlore structure, which involves superstructure. A typical SEM feature of the sintered compounds is shown in Fig. 5. It can be seen that the almost fully densified $LaGdZr_2O_7$ was obtained, and the grain size is about $1-5$ μm. The densities of the sintered specimens were higher than 96% of the theoretical values, according to the result of Archimedes drainage measurement.

B. Thermal conductivity

Thermal conductivity of the sintered specimen was measured by laser-flash method, and the composition dependency of the thermal conductivities of $(La_{1-x}Gd_x)_2Zr_2O_7$ ($0 \leqslant x \leqslant 1$) at different temperatures is shown in Fig. 6. It can be noticed that with increasing x, thermal conductivity of the solid solution first decreases, reaches a minimum value around x equal to 0.5, and then rises up to $x=1$. $LaGdZr_2O_7$, which exhibits the lowest thermal conductivity among all the

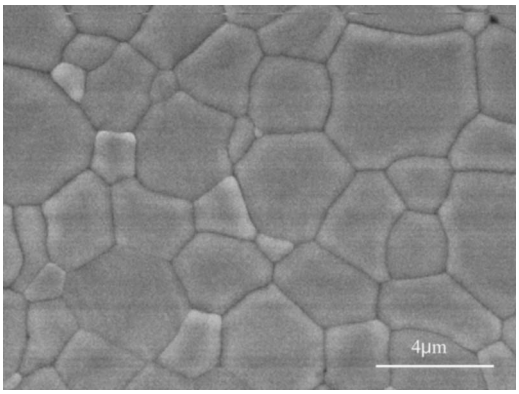

FIG. 5. SEM feature of the sintered $LaGdZr_2O_7$.

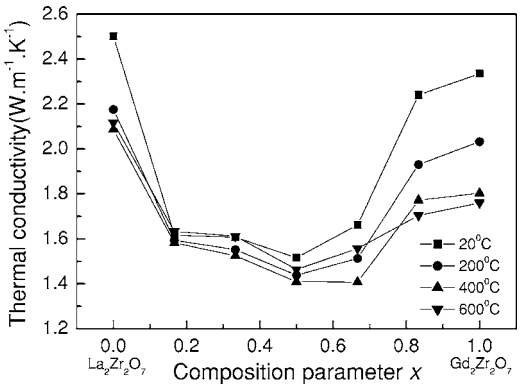

FIG. 6. Thermal conductivities of $(La_{1-x}Gd_x)_2Zr_2O_7$ at different temperatures.

compositions investigated, could be considered as a candidate in TBCs application. In Lehmann *et al.*'s work,[17] thermal conductivities of $La_2Zr_2O_7$ and $(La_{0.7}Gd_{0.3})_2Zr_2O_7$ at 600 °C have been determined to be 1.62 W/mK and 0.92 W/mK, which are quite different from the corresponding values of 2.1 W/mK and 1.53 W/mK in our work. The discrepancy arises mainly from large content of micropore (7%–31%) in the former work, which can decrease the net section of heat transportation[31] and reduce the thermal conductivity. In the present work, the effect of porosity has been properly erased by Eq. (2) as the porosity is less than 4%.

In the present study, the suppressed thermal conductivity of the solid solution may correlate with their point defects, that is, the substitution of La^{3+} with Gd^{3+} in $La_2Zr_2O_7$ or substitution of Gd^{3+} with La^{3+} in $Gd_2Zr_2O_7$. From the point of view of kinetic theory,[25] thermal transport in solids can be considered as the directional movement of phonon gas which carries energy. The thermal conductivity can be expressed as

$$K = \frac{1}{3} C_\nu \lambda \nu, \tag{4}$$

where C_ν, λ, and ν represent the heat capacity, phonon mean free path, and the mean velocity of phonons, respectively. In electrical-insulating solid, it is believed that the point defects affect the lattice vibrations and cause scattering for phonons owing to mass differences (mass fluctuation),[26,27] size and interatomic coupling force differences (strain field fluctuations),[28] which will shorten the mean free path of the phonon (λ). However, the effect of point defects on the velocity of the phonons (ν) and the heat capacity (C_P) has not yet been clarified and further investigation is needed.

C. Phonon mean free path

By substituting Eq. (1) and $C_P\rho = C_\nu$ in Eq. (4), the phonon mean free path could be expressed as

$$\lambda = 3\kappa/\nu. \tag{5}$$

The elastic wave velocity ν referred to the mean acoustic velocity and could be obtained by integration of the longitudinal (ν_p) and transverse (ν_s) wave velocities as[25]

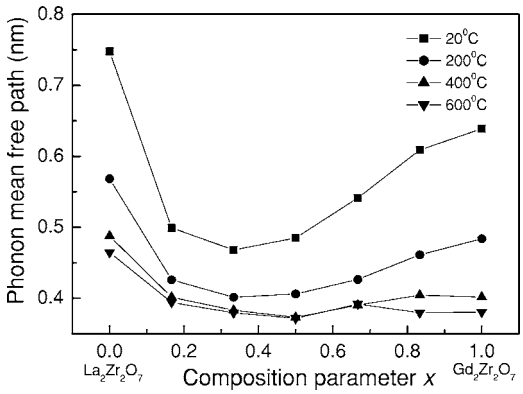

FIG. 7. Derived phonon mean free path of $(La_{1-x}Gd_x)_2Zr_2O_7$ at different temperatures.

$$\nu = 3^{1/3}\left(\frac{1}{\nu_P^3} + \frac{2}{\nu_S^3}\right)^{-1/3}. \quad (6)$$

The longitudinal and transverse wave velocities were directly measured by an ultrasonic instrument and the phonon mean free path could be eventually evaluated.

As shown in Fig. 7, all of the $(La_{1-x}Gd_x)_2Zr_2O_7$ solid solution investigated possess remarkably short phonon mean free paths, which are smaller than their respective lattice parameters ($\sim$1 nm). The results indicate the strong phonon scattering process in the crystal. The mean free path (λ) of a phonon in electrical-insulating solid under a certain frequency ω and temperature T can be approximately described by[17,29]

$$\frac{1}{\lambda(\omega,T)} = \frac{1}{\lambda_i(\omega,T)} + \frac{1}{\lambda_P(\omega,T)} + \frac{1}{\lambda_b}. \quad (7)$$

Here λ_i, λ_p, and λ_b represent the phonon mean free path corresponding with phonon Umklapp scattering, point defect scattering, and grain-boundary scattering processes, respectively. Since the mean free path of the phonon (λ) in this study is in the nanometer scale, the grain-boundary scattering could be omitted, due to the micrometer size grain of the sintered specimen in the present study. Therefore, the phonon mean free path is mainly restricted by phonon Umklapp scattering and point defect scattering processes. It can be found that the phonon mean free path decreases with increasing doping level from both sides of $La_2Zr_2O_7$ and $Gd_2Zr_2O_7$ due to enhancing point defect scattering strength. This effect seems less pronounced from the side of $Gd_2Zr_2O_7$, which could be attributed to the stronger Umkapp scattering in $Gd_2Zr_2O_7$. Lattice of $Gd_2Zr_2O_7$ must be more anharmonic than that of $La_2Zr_2O_7$, since the thermal expansion coefficient of $Gd_2Zr_2O_7$ (11.6×10^{-6} K^{-1}, 1100 °C) is apparently much larger than that of $La_2Zr_2O_7$ (9.0×10^{-6} K^{-1}, 1100 °C)[17]. With increasing temperature, the mean free path becomes less sensitive with the composition, which can be interpreted that Umklapp scattering increases with temperature and the relative importance of point defects is decreased at higher temperature. It is estimated that at high temperature, the phonon mean free path seems to approach a limit about 0.37 nm. Cahill *et al.*[30] and Clarke[31] have indicated that the minimum phonon mean free path should approach the distance between two neighboring atoms in the solid at high temperature. In the case of pyrochlore-type $(La_{1-x}Gd_x)_2Zr_2O_7$, the shortest interatomic distance can be roughly determined[16] by $a3^{1/2}/8$ from the lattice structure, where a represents the corresponding lattice constant. This expression gives an evaluation of the minimum phonon mean free path of these materials as small as 0.23 nm. Hence, it is believed that the rare-earth zirconate still has the potential in further reduction of thermal conductivity. Cahill *et al.*[30] has confirmed that simple, monatomic substitution (in this case La^{3+} by Gd^{3+}) could not produce sufficient phonon scattering sources to approach the lower thermal conductivity limit. Thus we proposed that substitution of both sites of rare-earth ions and Zr^{4+} simultaneously can introduce more phonon scattering sources and lead to a possible route for much lower thermal conductivities.

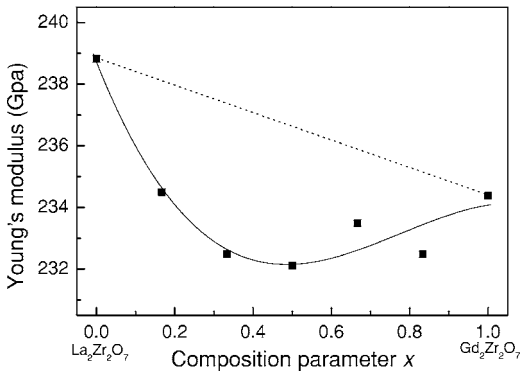

FIG. 8. Young's modulus of $(La_{1-x}Gd_x)_2Zr_2O_7$ specimens measured at room temperature.

D. Young's modulus

In solid solution, the strain field fluctuations induced by impurity atoms may alter the elastic properties, which could influence the phonon velocity and even the thermal transport property. Solute atoms entering the interstitial site always cause hardening of the crystal while the effect of substitutional atoms cannot be predetermined. Ibegazene *et al.*[32] substituted hafnia for zirconia in YSZ and resulted in progressive increase of Young's modulus of the solid solution, due to formation of new phase. In the present study, La^{3+} substituted by Gd^{3+} or Gd^{3+} displaced by La^{3+} did not create a new phase compared with the end compounds and reduced Young's modulus was observed. Figure 8 shows the Young's modulus of the solid solution at room temperature and the Young's moduli of all the solid solution are lower than those end compounds of $La_2Zr_2O_7$ and $Gd_2Zr_2O_7$. It can be inferred that the size and coupling force misfit induced by substitution atoms have "softened" the lattice and the strain field fluctuation results in lattice relaxation. The relaxation slows down the propagation velocity of phonons, which also suppresses the thermal conduction in the investigated solid solution. Clarke[31] deduced an expression for the thermal conductivity as

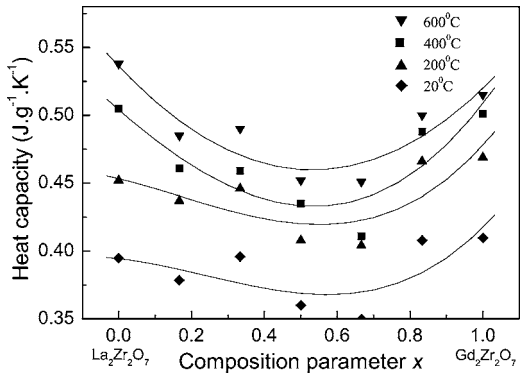

FIG. 9. Heat capacities of $(La_{1-x}Gd_x)_2Zr_2O_7$ specimens measured at different temperatures.

$$k \propto \frac{\rho^{1/6}E^{1/2}}{(M/m)^{2/3}}, \tag{8}$$

where ρ is the density, E represents the Young's modulus, M is the atomic weight of the molecule of the compound, and m is the number of atoms in the molecule. Equation (8) indicates that small value of E reflects a lower thermal conductivity, and it is also consistent with the results shown in Fig. 5. Besides, small Young's modulus is favored in TBC applications, as it produces smaller residual stresses in the coating system under the service conditions and results in better thermal-mechanical stability.[11,32,33]

E. Heat capacity

Equation (4) shows that the heat capacity C_P is also an important factor on the thermal conduction as C_P determines the carried energy of phonons. Up to now, only few studies of the thermodynamic properties of the lanthanide zirconate have been reported. Degueldre *et al.*[34] measured heat capacity of the solid solution of Er and Ce doping ZrO_2, Bolech *et al.*[35,36] studied the heat capacities of $La_2Zr_2O_7$ and $Ce_2Zr_2O_7$, and Lutique *et al.*[37] reported that of $Nd_2Zr_2O_7$. We measured the heat capacity of the $(La_{1-x}Gd_x)_2Zr_2O_7$ solid solution from 293 to 873 K using a DSC instrument. The data are shown in Fig. 9, and it can be seen that at a given temperature, the solid solution has lower heat capacities than those of $La_2Zr_2O_7$ and $Gd_2Zr_2O_7$ and the minimum value appears around the composition where x equals 0.5. Leitner *et al.*[38] has reviewed three empirical methods for the estimation of the relationship of standard molar heat capacity of mixed solid oxides with the composition. The Neumann-Kopp rule is the simplest and highly universal method for estimating heat capacity of the mixed oxide from the weighted sum of heat capacities of the constituent binary oxides, but in some cases the estimated accuracy will be reduced, and gives an error exceeding 5%.[38] It is obvious that the heat capacities results measured in the present study (Fig. 9) disobey the Neumann-Kopp rule. The minus deviation from Neumann-Kopp rule may come from the factor of structure, atomic, and ionic[39] contributions to the heat capacity of the solid solution. In present cases, the suppressed heat capacity of the solid solutions may be attributed to the enhanced anharmonicy aroused by the lattice distortion around the point defects

IV. DISCUSSION

A. Theoretical modeling of point defect scattering

In solid solution, the point defect scattering originates from both the mass difference (mass fluctuations) and the size and the interatomic coupling force differences (strain field fluctuations) between the impurity atom and the host lattice. Elastic continuum treatments, including Rayleigh's scattering theory and perturbation theory have been applied to describe the influence of point defects on the lattice thermal conductivity.[26,40,41] Here we present a phonon scattering model on the basis of the above theories and try to describe the effect of the composition of the solid solution on the thermal conductivity.

At temperature above the Debye temperature, the ratio of the lattice thermal conductivities of a material containing defects to that of the parent material can be written as[40]

$$\frac{k}{k_P} = \frac{\tan^{-1}(u)}{u}. \tag{9}$$

Here k and k_P are the lattice thermal conductivities of the defected and parent materials, respectively, and the parameter u is defined by[40]

$$u = \left(\frac{\pi^2\theta_D\Omega}{h\nu^2}k_P\Gamma\right)^{1/2}. \tag{10}$$

The letters h, ν, Ω, Θ_D stand for the Planck constant, lattice sound velocity, average volume per atom, and the Debye temperature. The imperfection scaling parameter Γ, representing the strength of point defects phonon scattering, always has two components, the scattering parameter due to mass fluctuations Γ_M and the scattering parameter due to strain field fluctuations Γ_S. Since their influences are additive, one writes $\Lambda=\Gamma_M+\Gamma_S$. In the available theoretical methods evaluating the thermal conductivity of solid solution,[28,42] Γ should be determined from measured thermal conductivity value, because of uncertainty of Γ_S. A phenomenological adjustable parameter ε is always included to obtain a fit between the theory and experimental values. However, in our theoretical approach, we made a direct estimation of ε and Γ from those relative physical properties and after adding temperature modification of the strength of point defect phonon scattering, we obtain perfect agreement between the calculated and measured values.

Supposing a compound U_xV_y, which has a crystal structure comprised of U and V sublattices and x, y are the relative degeneracies of the respective sites. As disorder may occur on both of the two sites, the total imperfection parameter Γ can be obtained by integration of the individual imperfection parameter of the constituted sublattices.[43]

$$\Gamma_{U_xV_y} = \frac{x}{x+y}\left(\frac{M_U}{M}\right)^2\Gamma_U + \frac{x}{x+y}\left(\frac{M_v}{M}\right)^2\Gamma_V, \tag{11}$$

where $M=(xM_U+yM_V)/(x+y)$, and M_U and M_V are the average mass of U and V sites, respectively. Γ_U and Γ_V repre-

sent the individual imperfection parameter of those two sites. For the pyrochlore-type solid solution $(La_{1-x}Gd_x)_2Zr_2O_7$, La and Gd are substituted for each other and there are four crystallographic sites, including the sites of (La,Gd), Zr,O and oxygen vacancy Vo, with their respective degeneracy of 2, 2, 7, 1, respectively. Then,

$$\Gamma_{(La_xGd_{1-x})_2Zr_2O_7} = \frac{2}{12}\left(\frac{M_{(La,Gd)}}{\bar{M}}\right)^2\Gamma_{(La,Gd)} + \frac{2}{12}\left(\frac{M_{Zr}}{\bar{M}}\right)^2\Gamma_{Zr} + \frac{7}{12}\left(\frac{M_o}{\bar{M}}\right)^2\Gamma_O + \frac{1}{12}\left(\frac{M_{V_O}}{\bar{M}}\right)^2\Gamma_{V_O}, \quad (12)$$

where $M_{(La,Gd)}$ is the average mass of the (La,Gd) sites and $\bar{M}$ is the average mass of $(La_{1-x}Gd_x)_2Zr_2O_7\square$, where $\square$ represents the oxygen vacancy and its mass is considered to be zero. Since there is no change on the sites of Zr, O and oxygen vacancy when the substitution between La and Gd occurs, $\Gamma_{Zr}=\Gamma_O=\Gamma_{VO}=0$, which gives

$$\Gamma_{(La_xGd_{1-x})_2Zr_2O_7} = \frac{1}{6}\left(\frac{M_{(La,Gd)}}{\bar{M}}\right)^2\Gamma_{(La,Gd)}. \quad (13)$$

In solid solution, the impurity atom differs from the host atoms in its mass, size, and the coupling force. Klemens[41] derived a generalized expression of the imperfection parameter taking these various factors into account

$$\Gamma_i = f_i\{(\Delta M_i/M)^2 + 2[(\Delta G_i/G) - 6.4\gamma(\Delta\delta_i/\delta)]^2\}. \quad (14)$$

Γ_i characterizes the scattering cross section of the impurity atom i, f_i is the fractional concentration of the impurity atom, M_i is the mass of impurity atom, M and δ are the mass and radius of the substituted site in the host lattice, δ_i is the radius of the impurity in the host lattice, G_i is an average stiffness constant of the nearest neighbor bonds from impurity to the host lattice, G is the corresponding quantity of the host atoms, $\Delta G_i=G_i-G$, $\Delta M_i=M_i-M$, $\Delta\delta_i=\delta_i-\delta$ and γ is the average anharmonicity of the bonds, namely, the Grüneisen parameter.

Here the term of $\Delta G_i/G$, which represents the influence of the coupling force misfit in $(La_{1-x}Gd_x)_2Zr_2O_7$, can be roughly estimated by comparing the Young's modulus of $La_2Zr_2O_7$ and $Gd_2Zr_2O_7$. Since the difference of the two compositions is no more than 2% from the Young's modulus data shown in Fig. 8, we omitted the contribution of coupling force misfit to strain field fluctuation, and Eq. (14) can be written as

$$\Gamma_i = f_i\{(\Delta M_i/M)^2 + 2[6.4\gamma(\Delta\delta_i/\delta)]^2\}. \quad (15)$$

According to the elastic continuum "sphere-in-hole" model,[44] the radius of the impurity atom will change when it enters a different lattice, depending on the elastic properties of the lattice. Eshelby derived the relation between the radius of impurity in its own lattice δ_i' and the corresponding value in the host lattice δ_i.[44]

$$\Delta\delta_i/\delta = [(\delta_i' - \delta)/\delta]p/(1+p), \quad (16)$$

where

$$p = (1+\nu)K_i/2K(1-2\nu). \quad (17)$$

K and ν are the bulk modulus and Poisson ratio of the matrix, respectively, and K_i is the bulk modulus of the impurity sphere. Here we also assumed that $K_i/K \approx 1$, for similar elastic properties of $La_2Zr_2O_7$, $Gd_2Zr_2O_7$ and their solid solution. Then substituting Eqs. (16) and (17) into Eq. (15), results in

$$\Gamma_i = f_i\left\{(\Delta M_i/M)^2 + 2\left[6.4\times\frac{1}{3}\gamma\frac{1+\nu}{1-\nu}(\delta_i' - \delta)/\ \delta)\right]^2\right\}. \quad (18)$$

Hereon we define the strain field factor ε

$$\varepsilon = \frac{2}{9}(6.4\times\gamma(1+\nu)/(1-\nu))^2 \quad (19)$$

yielding

$$\Gamma_i = f_i\{(\Delta M_i/M)^2 + \varepsilon[(\delta_i' - \delta)/\delta]^2\}. \quad (20)$$

Equation (20) is identical to Abeles's result,[26] but we give an expression of the parameter ε in Eq. (19), enabling direct prediction of imperfection scaling parameter Γ, as well as the thermal conductivity value of those solid solution with no fitting parameters.

For a mixture containing several different atoms, the total imperfection parameter is written as[26]

$$\Gamma = \sum_i \Gamma_i. \quad (21)$$

Then

$$\Gamma_{(La,Gd)} = \Gamma_{La} + \Gamma_{Gd} = x(1-x)[(\Delta M/M_{(La,Gd)})^2 + \varepsilon(\Delta\delta/\delta_{(La,Gd)})^2], \quad (22)$$

where

$$\Delta M = M_{La} - M_{Gd}, \quad (23)$$

$$\Delta\delta = \delta_{La}' - \delta_{Gd}', \quad (24)$$

and

$$M_{(La,Gd)} = xM_{La} + (1-x)M_{Gd}, \quad (25)$$

$$\delta_{(La,Gd)} = x\delta_{La}' + (1-x)\delta_{Gd}'. \quad (26)$$

Substituting Eq. (22) into Eq. (13), results in

$$\Gamma_{(La_xGd_{1-x})_2Zr_2O_7} = \frac{1}{6}\left(\frac{M_{(La,Gd)}}{\bar{M}}\right)^2 x(1-x)((\Delta M/M_{(La,Gd)})^2 + \varepsilon(\Delta\delta/\delta_{(La,Gd)})^2). \quad (27)$$

The term of $(\Delta M/M_{(La,Gd)})^2$ represents the contribution of mass fluctuations, while the term of $\varepsilon(\Delta\delta/\delta_{(La,Gd)})^2$ corresponds to the contribution of strain field fluctuations. From Eqs. (9), (10), (19), and (27), we can finally compute the thermal conductivity values of the investigated solid solution from that of their parent material, using those relative physical parameters which are already available in literature.

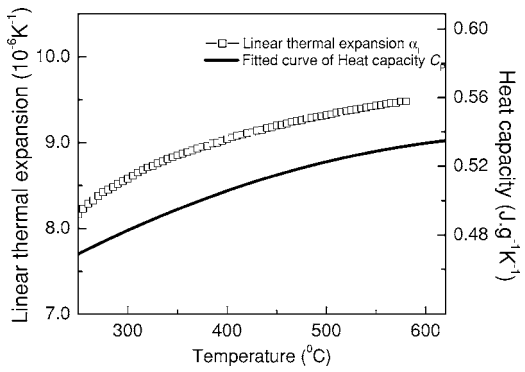

FIG. 10. Linear thermal expansion and heat capacity of $La_2Zr_2O_7$.

B. Determination of the parameters and calculation

In the present study, it is reasonable to assume $La_2Zr_2O_7$ rather than $Gd_2Zr_2O_7$ to be the parent material as the former possesses similar lattice structure with the solid solution. In Eq. (10), the parameters to be determined include the lattice sound velocity ν, average volume/atom Ω, and the Debye temperature Θ_D. ν has been calculated in Eq. (6) and the value of $La_2Zr_2O_7$ is 4165 m/s. Ω is given by M_A/ρ, where M_A is the average atomic mass and M_A of $La_2Zr_2O_7$ is 8.6×10^{-23} g. Then Ω for $La_2Zr_2O_7$ is 1.44×10^{-29} m^3. The Debye frequency ω_D is given[25] by $(6\pi^2\nu^3/\Omega)^{1/3}$, and the Debye temperature Θ_D is expressed as $\hbar\omega_D/k_B$, where $\hbar$ and k_B are Planck's and Boltzmann's constant, respectively. Accordingly, Θ_D of $La_2Zr_2O_7$ is estimated to be 510 K. In Eq. (24) and (26), δ'_{La} and δ'_{Gd} were determined as the ionic radius of La^{3+} and Gd^{3+} with eight coordination number (1.16 Å and 1.053 Å), as La^{3+} and Gd^{3+} occupy the eight-coordinate A site of the pyrochlore structure. For Eq. (19), we need to clarify the value of Poisson ratio ν and Grüneisen parameter γ. ν of $La_2Zr_2O_7$ is calculated to be 0.268 from the ultrasonic measurement. To make an accurate estimation of the Grüneisen parameter γ, we refer to the equation:[45]

$$\gamma = \alpha K/(C_V/V), \tag{28}$$

where α is the volume thermal expansion, which is three times of linear thermal expansion α_l. The bulk modulus K has been decided through ultrasonic measurement and K for fully dense $La_2Zr_2O_7$ is 171 GPa. C_ν (J mol^{-1} K^{-1}) is the specific heat at constant volume and V is molar volume. Considering that $C_\nu \approx C_P$ for solids, we use $C_P\rho$ to replace C_ν/V, as C_P here is given in unit of J g^{-1} K^{-1}. Equation (28) can be rewritten as

$$\gamma = 3\alpha_l K/(C_P\rho). \tag{29}$$

The thermal expansion data was obtained from the literature[46] and the curve of α_l versus C_P was plotted in Fig. 10. Relativity between the thermal expansion and heat capacity can be observed. The Grüneisen parameter γ of $La_2Zr_2O_7$ at 400 °C was estimated to be 1.54 from Eq. (29). The strain field factor ε was calculated to be 65 from Eq. (19). Hence, the imperfection scaling parameter Γ could be calculated, and the thermal conductivity values of the solid solution are able to be predicted from Equations (9) and (10). Here we just extrapolated the calculation to where the composition parameter x equals 0.9, as the solid solution in this area were expected to remain similar lattice properties of the host material $La_2Zr_2O_7$. Figure 11 shows the calculated results (the dashed curve) and the plots of experimental values at 400 °C.

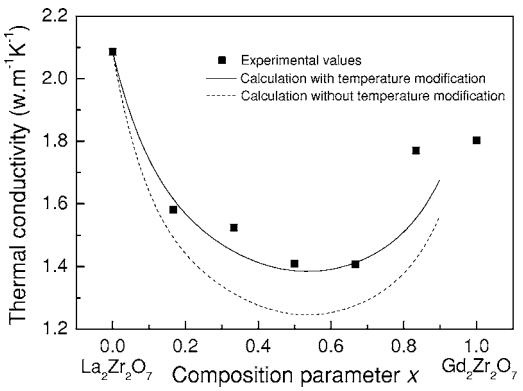

FIG. 11. Experimental thermal conductivity and theoretical calculation of $(La_{1-x}Gd_x)_2Zr_2O_7$ at 400 °C. (The calculation result without temperature modification is represented by the dashed curve and the solid curve represents the calculation result considering temperature modification.)

From Fig. 11, it can be found that the theoretical calculation describes well the trend of thermal conductivity with the variation of composition. However, the thermal conductivity values seem to be underestimated, which may be due to overestimation of phonon scattering strength by point defects.

C. Temperature modification

In the case of $(La_{1-x}Gd_x)_2Zr_2O_7$ solid solution, size misfit has become the dominant factor of strain field fluctuations, which distorts the lattice of the host material and scatters phonons. As temperature increases, the cell volume of the material expands, and the distortion induced is believed to be weakened, leading to attenuation of the phonon scattering by point defects. Meanwhile, the elastic properties of the bonds at high temperatures are different from those at room temperatures and the anharmocity may also be modified. Hence we made a careful temperature modification for the parameters we had used, in purpose of obtaining a better scaling of phonon scattering by point defects at high temperatures.

For many oxides, elastic properties have been identified to possess an approximate linear temperature dependency above room temperature.[47] We use the temperature coefficient of ZrO_2 offered in literature[48] as an approximation for that of $La_2Zr_2O_7$, that is 0.0645 GPa K^{-1} for Young's modulus and 0.0245 GPa K^{-1} for Shear modulus. Thus, the Young's modulus $E(T)$ and Shear modulus $\mu(T)$ of $La_2Zr_2O_7$ above room temperature can be written as

$$E(T) = E_0 - 0.0645(T - T_0), \tag{30}$$

$$\mu(T) = \mu_0 - 0.024(T - T_0), \tag{31}$$

where E_0 and G_0 represent Young's modulus (238.8 GPa) and Shear modulus (94.2 GPa) of fully dense $La_2Zr_2O_7$ at room temperature T_0 (25 °C).

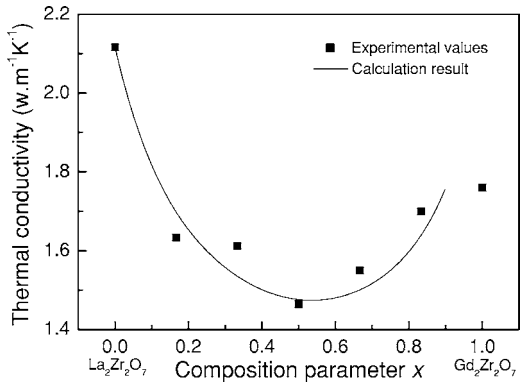

FIG. 12. Experimental thermal conductivity and theoretical calculation of $(La_{1-x}Gd_x)_2Zr_2O_7$ at 600 °C with temperature modification.

Then the Poisson ratio $\nu(T)$ and Bulk modulus $K(T)$ can be expressed.

$$\nu(T) = \frac{E(T)}{2\mu(T)} - 1, \tag{32}$$

$$K(T) = \frac{E(T)}{3(1-2\nu(T))}. \tag{33}$$

The Grüneisen parameter γ can be obtained by substituting Eq. (33) into Eq. (29) and the strain field factor $\varepsilon(T)$ was calculated by Eq. (19). At 400 °C, the parameters E, μ, ν, K, γ, and ε were determined to be 214.6 GPa, 85.2 GPa, 0.259, 148.4 GPa, 1.33, and 46, respectively. The theoretical calculation was conducted again and the result was plotted in Fig. 11 (described by the solid curve).

The calculation was found to be in good agreement with the experimental values, which validates our theoretical model. We also calculate the thermal conductivities of the solid solution at 600 °C and the parameters E, μ, ν, K, γ, and ε were determined to be 201.7 GPa, 80.4 GPa, 0.254, 136.7 GPa, 1.20, and 37, respectively. The result was plotted in Fig. 12.

The theoretical calculation still accounts well for the thermal conductivity values of the solid solution at 600 °C, which further supports our consideration in the model. However, with the same theoretical model, we failed to predict the exact thermal conductivity values of the solid solution using $Gd_2Zr_2O_7$ as the host material, which might be attributed to the difference in lattice structures of the solid solution and $Gd_2Zr_2O_7$.

In Wu *et al.*'s work,[12] a phonon-scattering model on basis of perturbation theory was used to describe the thermal conductivities of Gd_2O_3-ZrO_2 solid solutions. The effect of point defects of vacancies was well described in term of mass fluctuation, but the strain field fluctuation induced by point defects was not considered and an adjustable parameter was included, making this model semiempirical. Another case where perturbation theory applies is in Lehmann *et al.*'s effort[17] to calculate thermal conductivities of $La_2Zr_2O_7$ doped with 30 at. % of Nd, Eu, or Gd. Just like what we did in our model, this model has completely taken into account the scattering effects of point defects, including mass and bonding force differences of the substituted and substituting atoms, as well as the elastic field around a point imperfection. However, the Grüneisen parameter and elastic constants used in this model were all room temperature values, which would apparently change at high temperature. Hence, temperature dependence of these parameters should be considered to make this model more reasonable.

V. CONCLUSION

Thermal transport properties of single-phase $(La_{1-x}Gd_x)_2Zr_2O_7$ solid solutions have been investigated across the whole composition series. With increasing x, thermal conductivity of the solid solutions first decreases, reaches the minimum value when x equals to 0.5, and then rises up to $x=1$. $LaGdZr_2O_7$, which exhibits the lowest thermal conductivity, could be considered as a candidate in TBCs application. The point defect phonon scattering was identified as the main reason responsible for the reduced thermal conductivity of the solid solution. Due to lattice relaxation aroused by point defects, Young's modulus and heat capacities of the solid solution are suppressed, which also contribute to the reduction of thermal conductivity. A theoretical model on basis of elastic continuum theory has been developed to describe the influence of point defects on the lattice thermal conductivity by taking account of mass and strain field fluctuations. After adding temperature modification of the elastic properties, we obtain good agreement between the theory and experiment above the Debye temperature.

Our work has proved that forming solid solution on basis of an available material is an efficient way to achieve lower thermal conductivity while keeping other favorable properties in applications like TBCs. However, this effect is limited as the thermal conductivity of a solid cannot get below its amorphous limit and one feasible method is to introduce sufficient imperfection to approach this limit for a certain material system.

ACKNOWLEDGMENT

This work is financially supported by National Natural Science Foundation of China (Nos. 50232020 and 50572042).

*Corresponding author. FAX: +86 10 62771160. Email address: panw@mail.tsinghua.edu.cn

[1] D. R. Clarke and S. R. Phillpot, Mater. Today, **8**(6), 22 (2005).
[2] X. Q. Cao, R. Vassen, and D. Stoever, J. Eur. Ceram. Soc. **24**, 1 (2004).
[3] U. Schulz, C. Leyens, K. Fritscher, M. Peters, B. Saruhan-Brings, O. Lavigne, J. M. Dorvaux, M. Poulain, R. Mevrel, and M. L. Caliez, Aerosp. Sci. Technol. **7**, 73 (2003).
[4] N. P. Padture, M. Gell, and E. H. Jordan, Science **296**, 280 (2002).
[5] F. Cernuschi, P. Bianchi, M. Leoni, and P. Scardi, J. Therm. Spray Technol. **8**, 102 (1999).
[6] M. Fevre, A. Finel, and R. Caudron, Phys. Rev. B **72**, 104117 (2005).
[7] M. Fevre, A. Finel, R. Caudron, and R. Mevrel, Phys. Rev. B **72**, 104118 (2005).
[8] P. Strunz, G. Schumacher, R. Vassen, and A. Wiedenmann, Acta Mater. **52**, 3305 (2004).
[9] X. Chen, J. W. Hutchinson, and A. G. Evans, Acta Mater. **52**, 565 (2004).
[10] Q. Xu, W. Pan, J. D. Wang, C. L. Wan, L. H. Qi, H. Z. Miao, K. Mori, and T. Torigoe, J. Am. Ceram. Soc. **89**, 340 (2006).
[11] J. Wu, X. Z. Wei, N. P. Padture, P. G. Klemens, M. Gell, E. Garcia, P. Miranzo, and M. I. Osendi, J. Am. Ceram. Soc. **85**, 3031 (2002).
[12] J. Wu, N. P. Padture, P. G. Klemens, M. Gell, E. Garcia, P. Miranzo, and M. I. Osendi, J. Mater. Res. **17**, 3193 (2002).
[13] R. Vassen, X. Q. Cao, F. Tietz, D. Basu, and D. Stover, J. Am. Ceram. Soc. **83**, 2023 (2000).
[14] G. Suresh, G. Seenivasan, M. V. Krishnaiah, and P. S. Murti, J. Alloys Compd. **269**, L9 (1998).
[15] G. Suresh, G. Seenivasan, M. V. Krishnaiah, and P. S. Murti, J. Nucl. Mater. **249**, 259 (1997).
[16] P. K. Schelling, S. R. Phillpot, and R. W. Grimes, Philos. Mag. Lett. **84**, 127 (2004).
[17] H. Lehmann, D. Pitzer, G. Pracht, R. Vassen, and D. Stover, J. Am. Ceram. Soc. **86**, 1338 (2003).
[18] M. Maloney, U.S. Patent Nos. 6,177,200 (2001) and 6,231,991 (2001).
[19] J. D. Wang, W. Pan, Q. Xu, K. Mori, and T. Torigoe, Key Eng. Mater. **280-283**, 1503 (2005).
[20] C. L. Wan, W. Pan, Q. Xu, C. J. Jiang, K. Mori, and T. Torigoe, Key Eng. Mater. **280-283**, 1501 (2005).
[21] K. W. Schlichting, N. P. Padture, and P. G. Klemens, J. Mater. Sci. **36**, 3003 (2001).
[22] M. Asmani, C. Kermel, A. Leriche, and M. Ourak, J. Eur. Ceram. Soc. **21**, 1081 (2001).
[23] B. J. Wuensch, K. W. Eberman, C. Heremans, E. M. Ku, P. Onnerud, E. M. E. Yeo, S. M. Haile, J. K. Stalick, and J. D. Jorgensen, Solid State Ionics **129**, 111 (2000).
[24] L. Vegard, Z. Phys. **5**, 17 (1921).
[25] C. Kittle, *Introduction to Solid State Physics* (Wiley, New York, 1996).
[26] B. Abeles, Phys. Rev. **131**, 1906 (1963).
[27] G. A. Slack, Phys. Rev. **105**, 829 (1957).
[28] J. Yang, G. P. Meisner, and L. Chen, Appl. Phys. Lett. **85**, 1140 (2004).
[29] R. Berman, *Thermal Conduction in Solids* (Clarendon Press, Oxford, 1976).
[30] D. G. Cahill, S. K. Watson, and R. O. Pohl, Phys. Rev. B **46**, 6131 (1992).
[31] D. R. Clarke, Surf. Coat. Technol. **163**, 67 (2003).
[32] H. Ibegazene, S. Alperine, and C. Diot, J. Mater. Sci. **30**, 938 (1995).
[33] J. A. Thompson and T. W. Clyne, Acta Mater. **49**, 1565 (2001).
[34] C. Degueldre, P. Tissot, H. Lartigue, and M. Pouchon, Thermochim. Acta **403**, 267 (2003).
[35] M. Bolech, Thesis, University of Amsterdam, 1998.
[36] M. Bolech, E. H. P. Cordfunke, A. C. G. VanGenderen, R. R. VanderLaan, F. J. J. G. Janssen, and J. C. VanMiltenburg, J. Phys. Chem. Solids **58**, 433 (1997).
[37] S. Lutique, P. Javorsky, R. J. M. Konings, A. C. G. van Genderen, J. C. van Miltenburg, and F. Wastin, J. Chem. Thermodyn. **35**, 955 (2003).
[38] J. Leitner, P. Chuchvalec, D. Sedmidubsky, A. Strejc, and P. Abrman, Thermochim. Acta **395**, 27 (2003).
[39] P. J. Spencer, Thermochim. Acta **314**, 1 (1998).
[40] J. Callayway and H. C. von Baeyer, Phys. Rev. **120**, 1149 (1960).
[41] P. G. Klemens, Proc. Phys. Soc., London, Sect. A **68**, 1113 (1955).
[42] Z. Zhou, C. Uher, A. Jewell, and T. Caillat, Phys. Rev. B **71**, 235209 (2005).
[43] G. A. Slack, Phys. Rev. **126**, 427 (1962).
[44] F. Seitz and D. Turnbull, *Solid State Physics*, Vol. 3 (New York, 1956).
[45] G. Grimvall, *Thermophysical Properties of Materials* (Elsevier, Amsterdam, 1999).
[46] J. D. Wang, W. Pan, and Q. Xu, Rare Metal Mat. Eng. **34**, 581 (2005).
[47] J. B. Wachtman, W. E. Tefft, D. G. Lam, and C. S. Apstein, Phys. Rev. **122**, 1754 (1961).
[48] C. F. Smith and W. B. Crandail, J. Am. Ceram. Soc. **47**, 624 (1964).